ACES Asian Chemical Editorial Society

doi.org/10.1002/asia.202400408

CHEMISTRY AN ASIAN JOURNAL Research Article

www.chemasianj.org

Intercalated Water Drives Anomalous Thermal Expansion in the Tetragonal Zircon Structured Bismuth Vanadate $BiVO_4$ Photocatalyst

Bryce G. Mullens,[a] Frederick P. Marlton,[a, b] Maria K. Nicholas,[a] Ahmadi J. Permana,[a, c] Helen E. A. Brand,[d] Helen E. Maynard-Casely,[e] Philip A. Chater,[f] and Brendan J. Kennedy*[a]

The thermal transformation of the tetragonal-zircon (*tz*-) to tetragonal-scheelite (*ts*-)$BiVO_4$ was studied by *in situ* synchrotron X-ray diffraction, thermogravimetric analysis, and Fourier-transformed infrared spectroscopy. Upon heating, the tetragonal zircon polymorph of $BiVO_4$ (*tz*-$BiVO_4$) transitioned to the *ts*-polymorph between 693–773 K. Above 773 K, single phase *ts*-$BiVO_4$ was observed before transitioning to the monoclinic fergusonite (*mf*-) polymorph upon cooling. An anomaly in thermal expansion was observed between 400–500 K, associated with the loss of intercalated H_2O/NH_4^+ from the coprecipitation procedure. Heating *tz*-$BiVO_4$ resulted in contraction of the V–O bond distance and VO_4 polyhedra volume, ascribed to rotation of the tetrahedra groups. Attempts to study this by neutron diffraction failed due to the large incoherent scatter from the hydrogenous species. Efforts to remove these species while maintaining the *tz*-$BiVO_4$ structure were unsuccessful, suggesting they play a role in stabilizing the *tz*-polymorph. The local structure of both *mf*-BiVO4 and *tz*-BiVO4 were investigated by X-ray pair distribution function analysis, revealing local distortions.

Introduction

Solar-driven water splitting to produce sustainable hydrogen gas is likely to play a key role in addressing both energy security and environmental concerns during the transition to a carbon neutral economy. In the 50 years since Honda and Fujishima first used TiO_2 to produce hydrogen and oxygen gas through photocatalysis,[1,2] metal oxides have been extensively studied for photocatalytic water splitting. Bismuth vanadate ($BiVO_4$) is one of the most promising, and thus studied, oxides for photo- and electrocatalysis (PEC).[3–5] $BiVO_4$ exhibits other technologically important properties including ionic conductivity,[6,7] dielectric properties,[8,9] a ferroelastic-paraelastic phase transition,[10] and brilliant colors.[11] Owing to its very low toxicity and chemical stability, $BiVO_4$ is replacing toxic cadmium- and lead-based yellow pigments.[12–14]

$BiVO_4$ is polymorphic and three crystalline forms are found in nature, namely dreyerite, clinobisvanite, and pucherite. Dreyerite (Figure 1a) has a tetragonal zircon-type (*tz*) structure in space group $I4_1/amd$ (#141), and clinobisvanite (Figure 1c) has a monoclinic fergusonite-type (*mf*) structure in space group $I2/b$ (#15).[15] Synthetic analogues of both polymorphs are readily prepared, and the *mf*-structure can be obtained at room temperature by heating *tz*-$BiVO_4$ above 650 K.[16] Pucherite (Figure S1) is a rare mineral that has not been made in the laboratory, and exhibits an orthorhombic structure in space group *Pnca* (#60).[17] Heating *mf*-$BiVO_4$ to above 525 K results in a reversible transition to a tetragonal scheelite-type (*ts*) structure in space group $I4_1/a$ (#88, Figure 1b).[15,18] That the irreversible phase transition from *tz*- to *mf*-$BiVO_4$ is only observed for samples heated to above 650 K, which is above the *mf*-*ts* transition temperature,[16] strongly suggests that the *tz*-polymorph irreversibly converts to the *ts*-polymorph upon heating, and that the *ts*-polymorph reversibly transforms to the *mf*-polymorph upon cooling.

The structures of materials can be tuned by changing the size of the unit cell, as often observed in various variable temperature and pressure studies. In ABX_3 perovskites, symmetry lowering is often observed upon pressurizing as the rigid BX_6 octahedra cooperatively tilt to accommodate the smaller unit cell volume.[19,20] The opposite is observed upon heating,

[a] Dr. B. G. Mullens, Dr. F. P. Marlton, Ms. M. K. Nicholas, Mr. A. J. Permana, Prof. B. J. Kennedy
School of Chemistry, The University of Sydney, Sydney, New South Wales 2006, Australia
E-mail: brendan.kennedy@sydney.edu.au

[b] Dr. F. P. Marlton
Centre for Clean Energy Technology, School of Mathematical and Physical Sciences, Faculty of Science, University of Technology Sydney, Sydney, New South Wales 2007, Australia

[c] Mr. A. J. Permana
Department of Chemistry, Faculty of Science and Technology, Universitas Airlangga, Surabaya 60115, Indonesia

[d] Dr. H. E. A. Brand
Australian Synchrotron, Australian Nuclear Science and Technology Organisation, 800 Blackburn Road, Clayton, Victoria 3168, Australia

[e] Dr. H. E. Maynard-Casely
Australian Nuclear Science and Technology Organisation, Lucas Heights, New South Wales 2234, Australia

[f] Dr. P. A. Chater
Diamond Light Source, Harwell Science and Innovation Campus, Didcot, Oxfordshire OX11 0DE, United Kingdom

Supporting information for this article is available on the WWW under https://doi.org/10.1002/asia.202400408

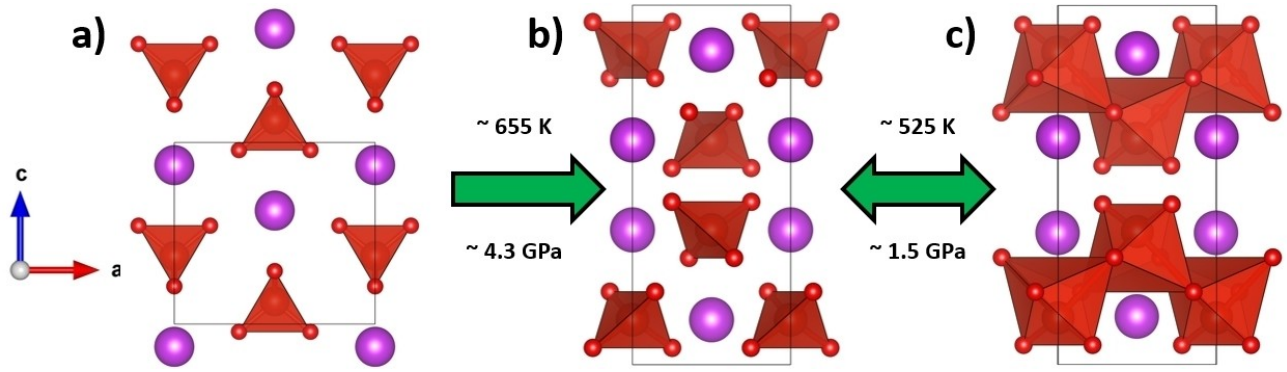

Figure 1. Three phases of $BiVO_4$. (a) The tetragonal-zircon form of space group $I4_1/amd$, (b) the tetragonal-scheelite form of space group $I4_1/a$, and (c) the monoclinic-fergusonite form of space group $I2/b$. Note that the monoclinic-fergusonite to tetragonal-scheelite phase transition is reversible with both temperature and pressure, whereas the tetragonal-zircon to tetragonal-scheelite phase transition is irreversible. In the figure, the large purple spheres represent the Bi^{3+} cations, the orange polyhedra represent either VO_4 or VO_6, and the small red spheres represent the oxygen anions.

where an increase in the unit cell volume and thermal motion can overcome energy-lowering phenomena such as Jahn-Teller distortions and octahedral tilting.[21] Phase transitions induced by either heating or pressurizing are often seen as opposites: with higher temperature favoring higher symmetry, and higher pressure favoring lower symmetry structures. The *tz*-$BiVO_4$ polymorph irreversibly transforms to the *ts*-polymorph under compression at 4.3(1) GPa at room temperature, with prolonged grinding of *tz*-$BiVO_4$ at room temperature also resulting in the formation of *mf*-$BiVO_4$.[16,22–24] *mf*-$BiVO_4$ is a unusual example of an oxide that *increases* in symmetry upon both pressurizing *and* heating. Application of either modest hydrostatic pressure (~1.5 GPa) at room temperature or modest heat (~525 K) induces the same *mf-ts* phase transition.[16,25] $BiVO_4$ has also been extensively studied using density functional theory (DFT), suggesting *mf*-BVO_4 spontaneously transforms to a higher-symmetry *ts*-BVO_4 phase contrary to the experimental observations. This discrepancy is thought to be related to the polarizability of the $Bi^{[3+]}$ ion.[26]

The three accessible phases of $BiVO_4$; *ts*-$BiVO_4$, *mf*-$BiVO_4$, and *tz*-$BiVO_4$, are all *n*-type semiconductors with band gap energies of 2.34, 2.40, and 2.90 eV respectively.[27,28] The band gap is between the valence band formed by the Bi 6*s* or a hybrid Bi 6*s* and O 2*p* orbital, and the V 3*d* conduction band.[29] The favorable band gap, together with the advantageous conduction band edge position and stability in aqueous media, contribute to the promising PEC properties of $BiVO_4$.[29] The *mf*-polymorph has been the most extensively studied as it has the highest photocatalytic activity for the oxygen evolution reaction.[30] Despite having the lowest photocatalytic activity due to its higher band gap ($E_g = 2.9$ eV), the *tz*-polymorph is of considerable interest as it can be prepared at low temperatures using solution-based methods.[30,31] The conduction band minimum (CBM) for these three phases is more positive than the H^+/H_2 reduction potential limiting its ability to generate H_2.[32–34]

The temperature dependence of the structures of both the *mf*- and *ts*-polymorphs of $BiVO_4$ have been widely studied, often focusing on the ferroelastic-paraelastic phase transition between them.[18,35] By comparison, relatively little is known about the temperature dependence of the structure of *tz*-$BiVO_4$, other than *ex situ* reports of its irreversible transformation to *mf*-$BiVO_4$.[24] However, there are numerous studies of the response of other oxides with the zircon structure to high temperature and/or high pressure.[36–38] While the high-pressure studies have revealed examples displaying displacive and/or reconstructive phase transformations, *tz*-$BiVO_4$ is a rare example of a zircon-structured material that undergoes a thermally induced reconstructive phase transition. In general, zircon-type ABO_4 oxides have low anisotropic thermal expansion that are very sensitive to the charge and size of the two cations. Patwe *et al.* concluded, from a comparative study of $LuPO_4$ and $LuVO_4$, that the thermal expansion in zircons is influenced by the distortion of the AO_8 polyhedra.[39] Correlated thermal motion associated with rigid BO_4 tetrahedra has been found to result in a reduction of the *B*–O bond distance in BO_4 tetrahedra with increasing temperature in other ABO_4 systems, including a number of scheelite type oxides.[40–42,43]

The effect of thermally induced vibrations on the structure of scheelites is currently of interest. It was recently demonstrated that thermally activated incoherent rotations of the rigid MoO_4 tetrahedra resulted in an unusual increase in the distortion of the CaO_8 polyhedra in $CaMoO_4$.[41] Similarly, incoherent translations were observed in the ReO_4 tetrahedra of $RbReO_4$ upon heating.[42] More dramatic changes occur in both $TlReO_4$ and $Bi(Fe_{0.67}Mo_{0.33})O_4$ associated with changes in the local ordering of the 6 s^2 lone pair electrons of the Tl^+ and Bi^{3+} cations,[44,45] as well as the Pb^{2+} lone pair distorting the WO_4 tetrahedra of $PbWO_4$.[46] *tz*-$BiVO_4$ is also a rare example of a zircon-structured material containing a cation with a potentially stereochemically active 6 s^2 lone pair of electrons and a nd^0 *B*-site cation, presenting possibilities of unique distorting behavior.

In situ synchrotron X-ray powder diffraction (SXRD) measurements of *tz*-$BiVO_4$ between 90 and 800 K are reported. The first objective of this present work was to confirm the hypothesis that the *tz*-polymorph irreversibly converts to the *ts*-polymorph upon heating and that this, in turn, transforms to the *mf*-polymorph form upon cooling. The role of water and

ammonium species was then elucidated using a combination of thermogravimetric analysis (TGA) and differential scanning calorimetry (DSC), coupled with Fourier-transformed infrared (FTIR) spectroscopy on the evolved gaseous species. Next, we sought to establish what, if any, role the Bi^{3+} 6s^2 lone pair electrons played in the thermal expansion of *tz*-$BiVO_4$. It is suggested that the lone pairs increase the susceptibility of the BiO_8 polyhedra to distort and this should be reflected in changes in the VO_4 polyhedra.

Experimental Methods

The *tz*-$BiVO_4$ polymorph was synthesized using a coprecipitation method. A Bi^{3+} solution (6.2 mmol, 10 mL) was prepared using $Bi(NO_3)_3 \cdot 5H_2O$ (Sigma-Aldrich, 98+%), and a V^{5+} solution (6.2 mmol, 50 mL) was prepared using NH_4VO_4 (The British Drug House, 98+%). These solutions were mixed whilst being heated at 60 °C, and NH_4OH (Merck, 3 M, 7.5 mL) was added dropwise until the solution turned a milky yellow color. NH_4OH (Merck, 3 M, 25 mL) was added quickly to elevate the pH, and the solution was vacuum filtered immediately and washed with deionized water. Further details on the synthesis are available in the electronic supporting information (ESI). The *mf*-$BiVO_4$ was synthesized by a solid-state reaction. Bi_2O_3 (Sigma-Aldrich, 99.9%) and V_2O_5 (Sigma-Aldrich, 99.6+%) were dried at 600 and 200 °C respectively for 16 hours before stoichiometric amounts (enough to synthesize 5 g of sample) were combined and hand ground in an agate mortar with acetone. The sample was pressed as a rod for 10 minutes at 20 MPa in a hydrostatic press before being heated to 750 °C for 24 hours in air in a muffle furnace.

Variable temperature TGA and DSC were performed using a Netzsch STA 449 F3 Jupiter. Four different samples were measured: $BiVO_4$ straight from the coprecipitation reaction, after heating at 100 °C for 1 hour, after heating at 600 °C for 1 hour, and after heating at 750 °C for 12 hours (confirmed to be *mf*-$BiVO_4$ by laboratory X-ray diffraction). Approximately 18 mg of each sample was weighed onto a platinum/rhodium pan with an Al_2O_3 liner and heated from 40–995 °C (~310 1270 K) at a rate of 10 K min^{-1} in dry air (80% N_2, 20% O_2) at 20 mL min^{-1}. The evolved gas was analyzed using a Bruker Vertex 80v spectrometer.

SXRD data were measured on the Powder Diffractometer BL-10 at the Australian Synchrotron (λ = 0.590067 Å, 21.0 keV) based on Rietveld refinement of a LaB_6 NIST SRM660B line profile standard.[47] This refinement, using the Thompson-Cox-Hastings profile function,[48] also supplied the instrument resolution function. The diffractometer uses an array of 16 Mythen II microstrip detector modules. To eliminate the gap between individual modules two datasets were collected with the detector assembly shifted by 0.5°. The resulting data sets were merged using bespoke software.[47] The sample was placed either in a 0.2 mm borosilicate glass capillary (for low temperature measurements) or was diluted with diamond powder and placed in a 0.5 mm quartz capillary for high temperature measurements. In both cases the capillary was rotated during the measurement to minimize preferred orientation effects. Temperature control was achieved using either an Oxford Cryosystems cryostream 700 or a hot air blower.

X-ray total scattering experiments were performed at beamline I15-1 of Diamond Light Source, UK (λ = 0.161669 Å, 76.69 keV). A small amount of the finely ground sample was loaded into a borosilicate glass capillary (inner diameter of 0.78 mm) to a height of 3.5 cm. Data were collected under ambient conditions for the sample, an empty capillary, and the empty instrument. Diffraction data were collected using two area detectors at different distances relative to the sample: 860 mm from the sample for Rietveld refinement, and 200 mm from the sample for X-ray pair distribution function (XPDF) analysis. Two dimensional diffraction data were corrected for the polarization, detector transmission, and flat field, with badly performing pixels masked prior to integration to one dimensional

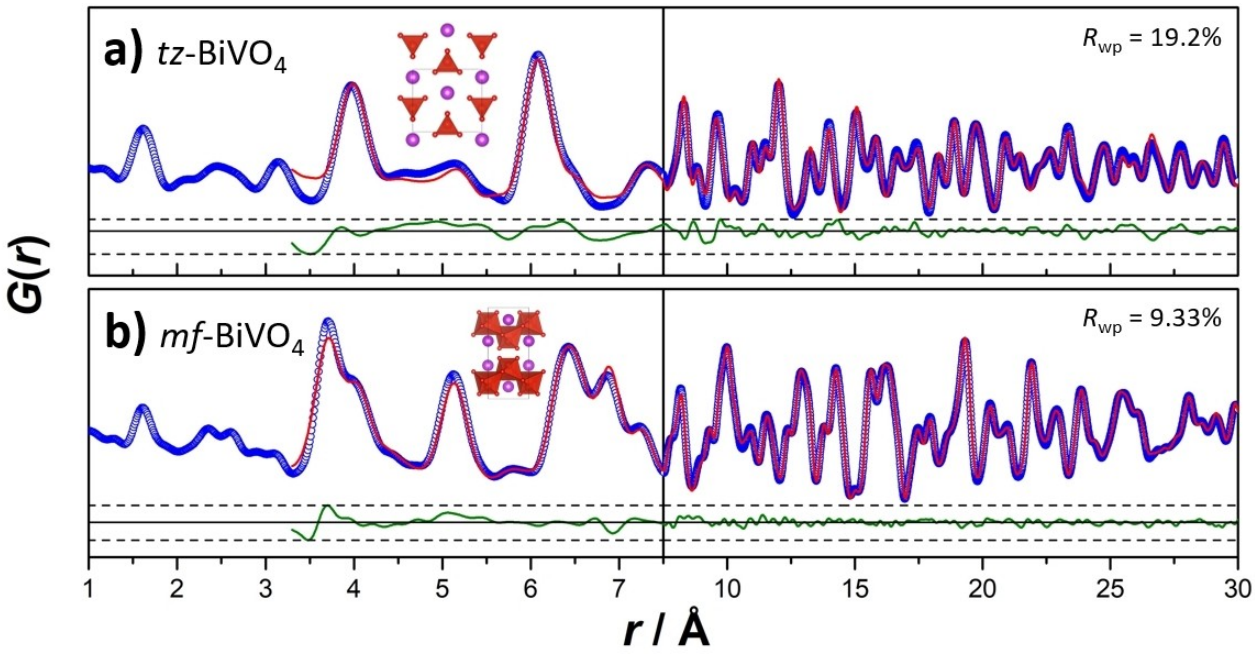

Figure 2. X-ray pair distribution function analysis of (a) tetragonal-zircon (*tz*-$BiVO_4$) and (b) monoclinic-fergusonite (*mf*-$BiVO_4$). The data has been fitted over a range of 3.3–30 Å, with the first half highlighting the fit from 3.3–7.5 Å, and the second half highlighting the fit from 7.5–30 Å. The blue circles represent the data, the red line represents the fit to the data, and the green line is the difference between the two. The insets show representations of the structure, where the purple spheres represent the Bi^{3+} cations and the V^{5+} cations are at the center of the orange polyhedra.

data using the program DAWN.[49] The XPDFs $G(r)$ were calculated using the PDFgetX3 software from the xPDFsuite with a Q_{max} of 25.0 (for *mf*-$BiVO_4$) and 17.4 (for *tz*-$BiVO_4$) $Å^{-1}$ respectively.[50,51]

Rietveld refinements against the SXRD and XPDF data were undertaken using the programs TOPAS6 and GSAS with the EXPGUI interface.[52–54] For the SXRD data, the background was modelled by a twelfth order shifted Chebyshev polynomial. The scale factor, lattice parameters, atomic coordinates, and atomic displacement parameters (ADPs) were refined simultaneously with the peak profile parameters. The Rietveld refinements were performed sequentially, with the structure updated after each refinement. The sequential refinements were undertaken starting from both the low and high temperature regions for the data measured upon heating. In the final refinement cycles, the profile and lattice parameter were released, and no constraints were placed on either the atomic coordinates nor atomic displacement parameters. Structural illustrations were drawn using the program VESTA.[55]

Results and Discussion

Room Temperature Structure of tz- and mf-$BiVO_4$ Using Synchrotron X-Ray Diffraction

The SXRD data for the as-prepared sample of *tz*-$BiVO_4$ measured at 300 K was well fit using the tetragonal zircon model described previously, and the refined structural parameters showed good agreement with the literature (Figure S3a).[16,56] The SXRD data for the *mf*-$BiVO_4$ sample measured at 300 K was well fit using the monoclinic fergusonite-type model, and was also in good agreement with published values (Figure S3b).[15,57] The *tz*-$BiVO_4$ structure consists of chains of edge-sharing BiO_8 dodecahedra along both the *a*- and *b*-axes, joined by isolated VO_4 tetrahedra. At 300 K, the BiO_8 dodecahedra have two different Bi–O lengths of 2.481(4) and 2.502(4) Å, and a unique V–O bond length of 1.625(4) Å. The VO_4 tetrahedra are not regular but are best described as tetragonal disphenoid as evident from the O–V–O bond angles of 99.0(3) and 114.94(14)°. The *mf*-$BiVO_4$ structure consists of similar chains of edge-sharing BiO_8 dodecahedra along the *b*- and *c*-axes joined

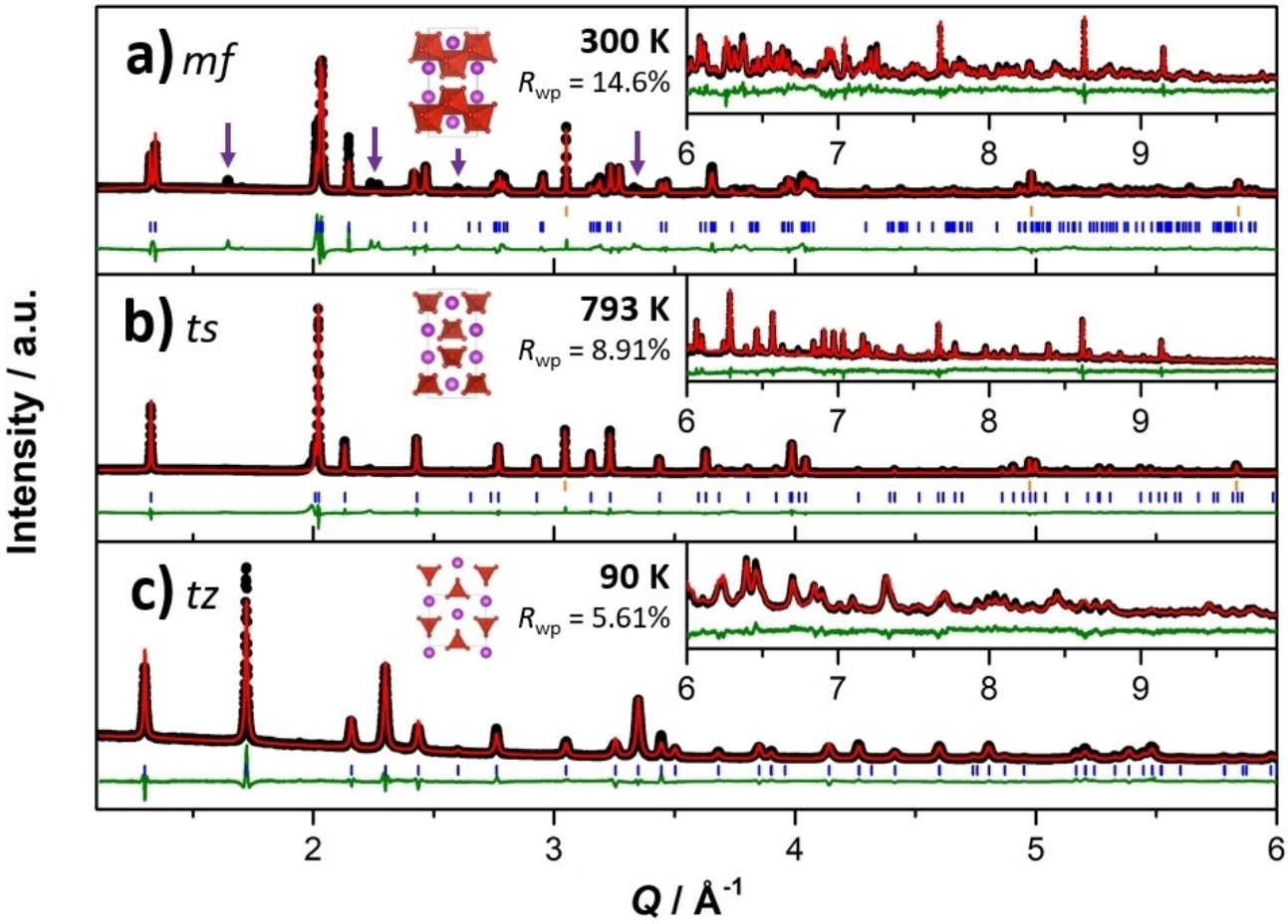

Figure 3. Rietveld refinements for $BiVO_4$ using synchrotron X-ray powder diffraction at (a) 300 K upon cooling, fitted to the monoclinic-fergusonite *I*2/*b* model, (b) 793 K fitted to the tetragonal-scheelite $I4_1/a$ model, and (c) 90 K fitted to the tetragonal-zircon $I4_1/amd$ model. The black circles represent the data, the red lines represent the calculated profile, the green lines represent the difference between the data and the calculated profile. The orange and blue tick marks are the space group-allowed reflections of the diamond ($Fd\bar{3}m$) and the respective $BiVO_4$ phase. The purple arrows in (a) show the reflections of the decomposed Bi_2SiO_5 phase. The insets show representations of the structure, where the purple spheres represent the Bi^{3+} cations and the V^{5+} cations are at the center of the orange polyhedra.

by isolated VO_4 tetrahedra. However, the BiO_8 dodecahedra are arranged slightly differently, leading to a smaller unit cell parameter by a factor of $1/\sqrt{2}$. The near equality of the Bi–O distances in the BiO_8 polyhedra of *tz*-$BiVO_4$ is similar to that described for the *ts*-polymorph,[58] and implies there is no long-range ordering of the Bi^{3+} 6 s^2 lone pair electrons. This contrasts with *mf*-$BiVO_4$, where the stereochemical activity of the Bi^{3+} 6 s^2 lone pair electrons cause the Bi^{3+} cations to offset along the *c*-axis resulting in four different Bi–O bond lengths and a distortion of the BiO_8 polyhedra.

The distortion of the BiO_8 polyhedra in *tz*-$BiVO_4$ observed here is noticeably less than that described in the earlier single crystal study of a naturally occurring sample by Dreyer and Tillmanns,[56] who reported distances of 2.414 and 2.549 Å. The *c*-axis described in the literature is noticeably longer than observed here [6.584(3) Å *vs.* 6.46260(13) Å],[24] and this may be the cause of the difference in bond distance anisotropy. Surprisingly, comparable bond length distortions in the AO_8 polyhedra are observed in other vanadium zircons, such as $GdVO_4$ [2.36(1) and 2.49(1) Å], and $LuVO_4$ [2.262(8) and 2.431(5) Å],[39,59–61] suggesting the Bi^{3+} 6 s^2 lone pair is inert and exhibits little stereochemical activity in the *tz*-$BiVO_4$ structure. This has been seen in similar metal oxyhalide structures, where Bi^{3+} can 'deactivate' its 6 s^2 lone pair to lower its overall energy and accommodate high symmetry sites.[62] The V–O distances of 1.68(1) and 1.687 Å in $GdVO_4$ and $LuVO_4$ are comparable to the distance of 1.625 Å observed here at room temperature, which is significantly shorter than reported by Dreyer and Tillmanns (1.703 Å) or Sánchez-Martín *et al.* (1.686 Å).[16,56]

To further understand the difference in structure between both room temperature $BiVO_4$ polymorphs, X-ray pair distribution function (XPDF) was analyzed for both *tz*- and *mf*-$BiVO_4$ (Figure 2). Analysis of the two datasets at room temperature across the 1.2-30 Å range resulted in poor fits due to the weak scatter of X-rays by the oxygen anions (Figures S4–5). To minimize the impact of this, a reduced fitting range of 3.3–30 Å was used, meaning the immediately correlated Bi–O and V–O bonds were not modelled and only the cation-cation distances were captured. Small box fits (a.k.a. real space Rietveld refinement) of *tz*-$BiVO_4$ using the same structural model derived from the SXRD data at 300 K show a relatively poor fit to the data. Although the significant peaks are fit, there is a large amount of residual observed indicating the model is not an accurate depiction of the structure. The *mf*-$BiVO_4$ structural model returns a much better fit to the data, with small residuals observed both at low and at high *r*.

A significant difference between the *tz*- and *mf*-$BiVO_4$ structures is that the *mf*-$BiVO_4$ model accounts for the stereochemistry of the Bi^{3+} 6 s^2 lone pair, whereas the *tz*-$BiVO_4$ does not. In *mf*-$BiVO_4$ the BiO_8 polyhedra contain four different Bi–O bonds, reflecting displacement of the Bi^{3+} cations along the *c*-axis. In the *tz*-$BiVO_4$ structure, no such freedom exists, and in this structure the Bi^{3+} cations are at the symmetry constrained 4*a* (0, 3/4, 1/8) Wyckoff position. Further, as demonstrated by infrared studies,[63] samples of *tz*-$BiVO_4$ can also contain a large amount of interstitial water and ammonium species, which can also contribute to the poor XPDF fit. Although H_2O and NH_4^+ do not strongly scatter with X-rays, their presence within the *tz*-$BiVO_4$ structure may cause local distortions including displacement of either Bi^{3+} or V^{5+} cations from their symmetry constrained Wyckoff positions to lower symmetry positions. This could lead to flexibility within the cation-cation distances of the *tz*-$BiVO_4$ structure that is not captured by the apparent structural model.

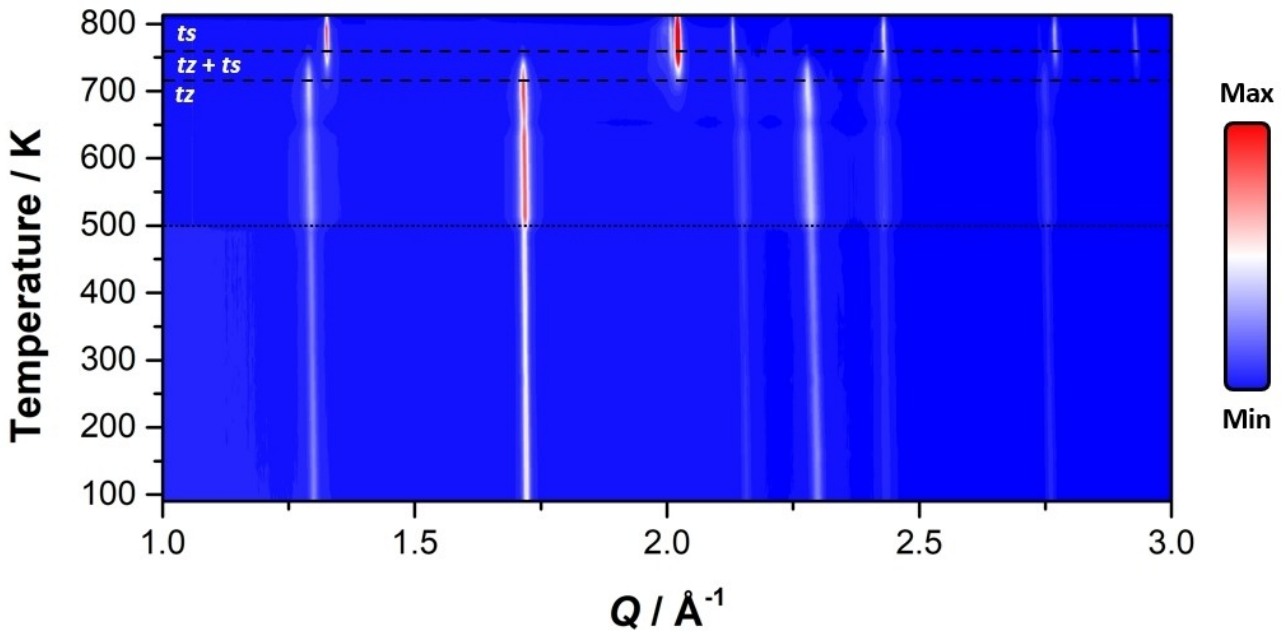

Figure 4. Temperature dependent synchrotron X-ray diffraction patterns of tetragonal-zircon $BiVO_4$ measured on heating from 90–800 K. The $I4_1/amd$ and $I4_1/a$ two-phase region is shown within the two dashed lines. The change in peak widths around ~500 K, indicated by the dotted line, is due to a change in the sample capillary used and the heating environment. The data were collected at $\lambda = 0.590067$ Å.

Variable Temperature Behavior of tz-$BiVO_4$ Using Synchrotron X-Ray and Neutron Diffraction

The temperature dependence of the structure of *tz*-$BiVO_4$ was determined using SXRD (Figure 3 and S6). Preliminary measurements, where the sample was contained in a 0.2 mm diameter quartz glass capillary, revealed that it reacted with the capillary at high temperatures, causing the capillary to fail. To minimize the contact between the sample and the capillary, it was elected to use a relatively large diameter capillary (0.5 mm diameter), with X-ray absorption by the sample minimized by mixing it with an equal volume of diamond powder. This allowed measurements to be undertaken to 793 K. As illustrated in Figure 4, the sample remained single phase (*tz*) to around 693 K, at which point additional reflections due to the formation of the *ts*-polymorph began to form. These two phases coexisted over a relatively wide temperature range (Figure S7), but at $\geq$773 K the only crystalline phase observed was the *ts*-polymorph. At 793 K the BiO_8 polyhedra of the *ts*-polymorph are more distorted than in the *tz*- counterpart [Bi–O = 2.494(9) and 2.575(9) Å], and the VO_4 tetrahedra are less strained [O–V–O = 106.5(3) and 115.7(7)°]. There is no indication from the diffraction data that the *mf*-polymorph forms during the heating of the *tz* phase, verifying the hypothesis that the *tz*-polymorph directly transforms to the *ts*-polymorph. The sample was then cooled to room temperature where an additional diffraction pattern was collected. The cooled dataset was fit to the *mf*-$BiVO_4$ model that has a more distorted BiO_8 polyhedra [four different Bi–O distances ranging from 2.380(11)-2.818(14) Å] than either of the tetragonal polymorphs and a distorted VO_4 tetrahedra with two different bond distances [V–O = 1.488(14) and 1.761(11) Å]. In addition to the expected *mf*-$BiVO_4$ phase, the formation of Bi_2SiO_5 (~19.5 wt%) was also observed together with some broad features that are presum-

Table 1. Selected Rietveld refinement structural parameters, bond distances, and bond angles for $BiVO_4$ using synchrotron X-ray diffraction data.

Temperature (K)		90	300 (Heating)	793	300 (Cooled)
Space Group		$I4_1/amd$	$I4_1/amd$	$I4_1/a$	$I2/b$
a (Å)		7.29455(11)	7.30500(12)	5.17018(5)	5.19312(9)
b (Å)		= a	= a	= a	5.09432(9)
c (Å)		6.44174(12)	6.46257(13)	11.80043(13	11.7018(2)
γ (°)		= 90	= 90	= 90	90.3498(11)
Volume (Å^3)		342.768(12)	344.863(13)	315.434(7)	309.570(9)
Bi	x	= 0	= 0	= 0	= 0
	y	= 3/4	= 3/4	= 1/4	= 1/4
	z	= 1/8	= 1/8	= 5/8	0.63518(13)
V	x	= 0	= 0	= 0	= 0
	y	= 1/4	= 1/4	= 1/4	= 1/4
	z	= 3/8	= 3/8	= 1/8	0.1251(5)
O(1)	x	= 0	= 0	0.1343(18)	0.156(2)
	y	0.0799(5)	0.0808(5)	0.4856(15)	0.4781(18)
	z	0.2093(5)	0.2117(5)	0.1997(8)	0.2150(10)
O(2)	x	–	–	–	0.302(2)
	y	–	–	–	0.344(3)
	z	–	–	–	0.4570(13)
Bi–O		2.467(4)	2.481(4)	2.494(9)	2.380(11)
Bi–O		2.485(4)	2.502(4)	2.575(9)	2.440(11)
Bi–O		–	–	–	2.651(14)
Bi–O		–	–	–	2.818(14)
BiO_8 (Å^3)		27.4	27.8	29.6	29.8
V–O		1.637(4)	1.625(4)	1.656(9)	1.488(14)
V–O		–	–	–	1.761(11)
VO_4 (Å^3)		2.19	2.15	2.26	2.12
O–V–O		98.6(3)	99.0(3)	106.5(3)	99.6(12)
O–V–O		115.17(14)	114.94(14)	115.7(7)	106.4(7)
$B_{eq.}$ (Bi) (Å^2)		0.633(12)	1.166(16)	2.05(3)	1.18(3)
$B_{eq.}$ (V) (Å^2)		0.27(4)	0.47(5)	1.09(8)	0.36(8)
$B_{eq.}$ (O) (Å^2)		0.19(8)	0.40(9)	0.6(2)	3.7(4)
R_{wp} (%)		5.50	5.35	8.83	9.74

ably are due to a poorly crystalline vanadium oxide. These are summarized in Table 1.

Examination of the thermal expansion of the unit cell parameters for *tz*-$BiVO_4$ reveals a small anomaly around 400 K, which is most noticeable in the *a* lattice parameter and the ADPs. The *tz*-$BiVO_4$ phase undergoes linear thermal expansion until this temperature, where a change in the rate of thermal expansion is evident. The linear thermal expansion coefficients (TEC) for *tz*-$BiVO_4$ between 90 and 713 K were estimated using $\alpha_P = \frac{\Delta P}{P_i \Delta T}$ where P_i is the parameter of interest and ΔT is the change in temperature. These were calculated as $\alpha_a = 5.8\times10^{-6}$ Å K^{-1}, $\alpha_c = 17.4\times10^{-6}$ Å K^{-1} and $\alpha_{Vol.} = 31.6\times10^{-6}$ Å^3 K^{-1}. These values are in reasonable agreement with the values reported for various other *Ln*VO_4 zircon structures ($\alpha_a = 0.7$–8.7×10^{-6} Å K^{-1} and $\alpha_c = 3.2$–14.1×10^{-6} Å K^{-1}). It is possible that the anomaly around 400 K (~125 °C) is related to the loss of water and/or ammonium species trapped during the coprecipitation procedure. The ADPs are presented in Figure 5d and show unusual behavior with the heavier Bi^{3+} cations exhibiting greater thermal motion than the lighter V^{5+} cations and oxygen anions. This has been observed in previous studies, with abnormally high ADPs used to account for the displacement of cations with stereochemically-active lone pairs in the long-range average structure, such as Pb^{2+} in $Pb(Ti_{1-x}Zr_x)O_3$ and PbTe.[64–66] As seen in the XPDF results of *tz*-$BiVO_4$, the Bi^{3+} cation is presumed to sit away from the center of the BiO_8 polyhedra due to the stereochemistry of the Bi^{3+} 6 s^2 lone pair, leading to an increase in the ADP modelled using Rietveld refinement.

The high energy and low d_{min} (< 0.45 Å) probed using SXRD means that very precise values of both the cation and anion atomic coordinates were obtained. As a result, accurate Bi–O and V–O bond distances were extracted from the refinements. The temperature dependencies of the Bi–O and V–O bond distances are shown in Figure 6. The Bi–O distances, as expected, expand upon heating noting the small deviation from linear behavior above ~500 K. This correlates with the small anomalies in the thermal expansion of the unit cell parameters and is believed to have the same origin, namely the loss of H_2O and NH_4^+ species upon heating. Surprisingly, the V–O distance decreases upon heating to around 550 K, above which they increase. Such anisotropy in the *A*-O and *B*-O bond lengths in zircon materials has previously been observed in materials exhibiting anomalous thermal expansion behavior.

Negative thermal expansion (NTE) behavior has been observed $A(BO_4)_2$ and $\mathbf{A}_2(\mathbf{B}O_4)_3$ (B^{6+} = Mo, W) oxides that, like $BiVO_4$, contain a small *A*-site cation and approximately rigid BO_4 tetrahedra.[40,67–69] Such NTE is a consequence of transverse vibrations of bridging oxygen atoms associated with rotation of the BO_4 tetrahedra. Although the *Ln*VO_4 zircon vanadates do not show NTE, Chakoumakos *et al.* previously established that the oxygen displacement in these are highly anisotropic with the maximum vibration amplitude perpendicular to the edge shared between the VO_4 tetrahedra and the *Ln*O_8 polyhedra.[60]

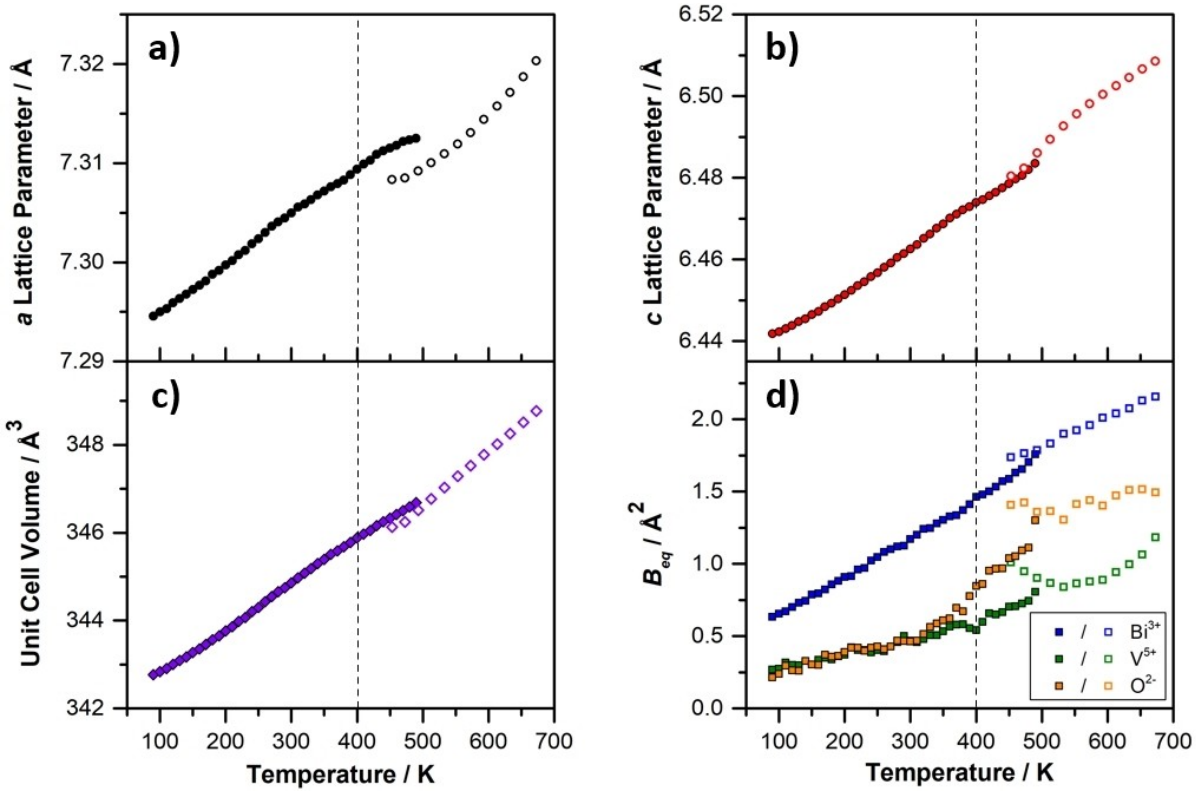

Figure 5. Temperature dependence of the (a,b) unit cell parameters, (c) unit cell volume, and (d) the atomic thermal parameters. The solid symbols are derived from the cryostream, whereas the hollow symbols are derived from the hot air blower. The dotted line is drawn to highlight the anomalies above 400 K. The discontinuity in (a) is an experimental artifact associated with the loss of water and the need to change sample environment from the cryostream to the hot air blower.

We propose that an increase in such transverse vibrations upon heating could result in the observed apparent reduction in the V–O bond lengths. A similar effect has been observed in some scheelite-type oxides, where a shortening on the *B*-O bonds observed in Rietveld refinement was related to local incoherent translations and rotations of the rigid tetrahedra units.[42,70, 43]

The presence of interstitial species within the *tz*-$BiVO_4$ structure has not been well explored previously. When attempting to collect neutron powder diffraction (NPD) data on a freshly prepared sample of *tz*-$BiVO_4$, a large background was evident. This was presumably the result of incoherent scatterer from H_2O and/or NH_4^+ species trapped within the coprecipitated sample of *tz*-$BiVO_4$; recall that hydrogen is a large incoherent neutron scatterer (Figure S9). An experiment was attempted where the water was removed by heating *in situ* with an ILL-type vacuum furnace. This resulted in a decrease in the background and additional reflections diagnostic of the *ts*-$BiVO_4$ phase emerging (Figure S10). This suggests that the presence of H_2O and NH_4^+ species may stabilize the *tz*-$BiVO_4$ structure, and removal of these facilitates the *tz*-*ts* transformation. As noted above, the small anomaly in the unit cell parameters observed in the variable temperature SXRD data (Figure 5a) is believed to be a consequence of the loss of such species.

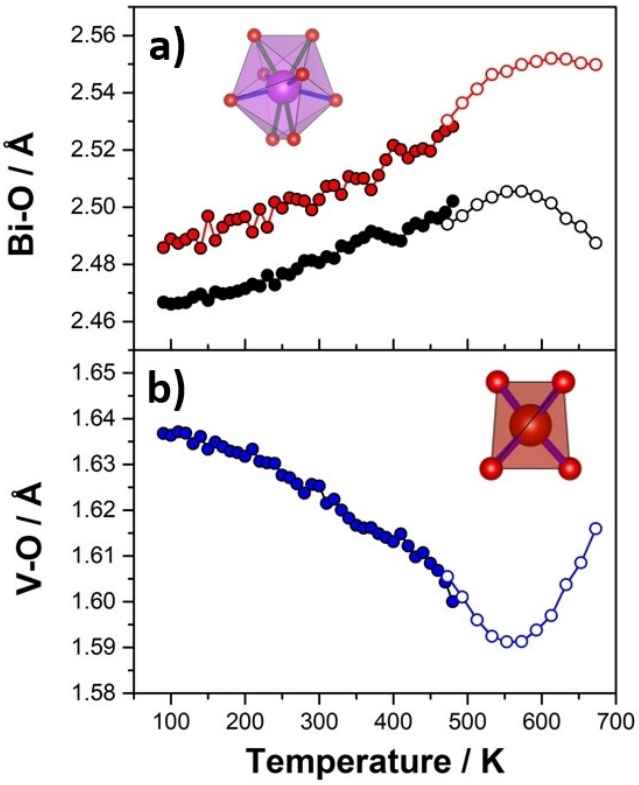

Figure 6. Temperature dependence of the (a) Bi–O and (b) V–O bond distances for *tz*-$BiVO_4$ estimated from Rietveld refinements against synchrotron X-ray diffraction data. The solid symbols are derived from the cryostream, whereas the hollow symbols are derived from the hot air blower. The insets illustrate the polyhedra environments, with (a) showing the BiO_8 polyhedra where the large purple sphere represents Bi^{3+}, and with (b) showing the VO_4 polyhedra where the large orange sphere represents V^{5+}. In both cases, the bond lengths are color-coded in terms of length, and the red spheres represent oxygen.

Variable Temperature Thermogravimetric Analysis and Fourier-Transformed Infrared Spectroscopy

To investigate the presence of these species within the coprecipitated sample of *tz*-$BiVO_4$, room temperature FTIR spectra were collected on four differently treated samples: straight from the coprecipitation reaction, heated at 100 °C for one hour, heated at 600 °C for one hour, and heated at 750 °C for 12 hours (Figure S12). The final sample is *mf*-$BiVO_4$, as confirmed by laboratory X-ray diffraction. The infrared spectra confirmed that water was present in both the coprecipitated sample, and the sample heated at 100 °C, as evident by the presence of an O–H stretch band at ν ~3250 cm^{-1} and an O–H bend at ~1380 cm^{-1}. Additional species also appear to be present based on the absorbance at ~1300–1600 cm^{-1}, most likely associated with either CO_2 or remaining ammonium species. These bands were absent in the samples heated to higher temperatures, indicating that the species responsible can be removed by heating.

The undried sample of *tz*-$BiVO_4$, from the coprecipitation synthesis, was also analyzed using variable temperature TGA/DSC with an FTIR attachment. This allows for the correlation between the loss of sample mass, and the identification of the species that had been released. The TGA/DSC is shown in Figure 7 (with TGA/DSC and FTIR shown on two other samples in Figures S12–13). A significant drop in mass of ~26% is observed between room temperature and ~130 °C (~400 K) associated with the loss of adsorbed water. An additional ~2% drop in mass is observed at ~250 °C (~525 K) and this has previously been attributed to the loss of surface hydroxyl group and remaining ammonium or nitrate ions from the coprecipitation reaction.[30,71–73] There is a continuous loss in mass between 270–420 °C (~425-695 K) that correlates with the appearance of both O–H and N–H bends in the FTIR, indicating further elimination of H_2O and NH_4^+ species. Yu *et al.* had previously attributed a TGA feature between 483–653 K to the crystallization of *ts*-$BiVO_4$.[30] Our SXRD results show this not to be the case as the *ts*-$BiVO_4$ phase does not form until $>$693 K. The TGA/DSC data for $BiVO_4$ after being heated to 750 °C (1023 K) for 12 hours showed no significant variation in mass nor evidence for detected species in the FTIR (Figures S12–13). It is postulated that the strongly bonded H_2O and NH_4^+ species assist in stabilizing the *tz*-$BiVO_4$ phase at room temperature.

Conclusions

The thermally induced tetragonal-zircon to tetragonal-scheelite transformation in $BiVO_4$ has been studied using *in situ* X-ray diffraction methods complemented by a combined TGA/FTIR analysis. Upon heating, *tz*-$BiVO_4$ undergoes a first order reconstructive phase transition to the *ts*-$BiVO_4$ polymorph over a relatively wide temperature range of 693–773 K. Upon cool-

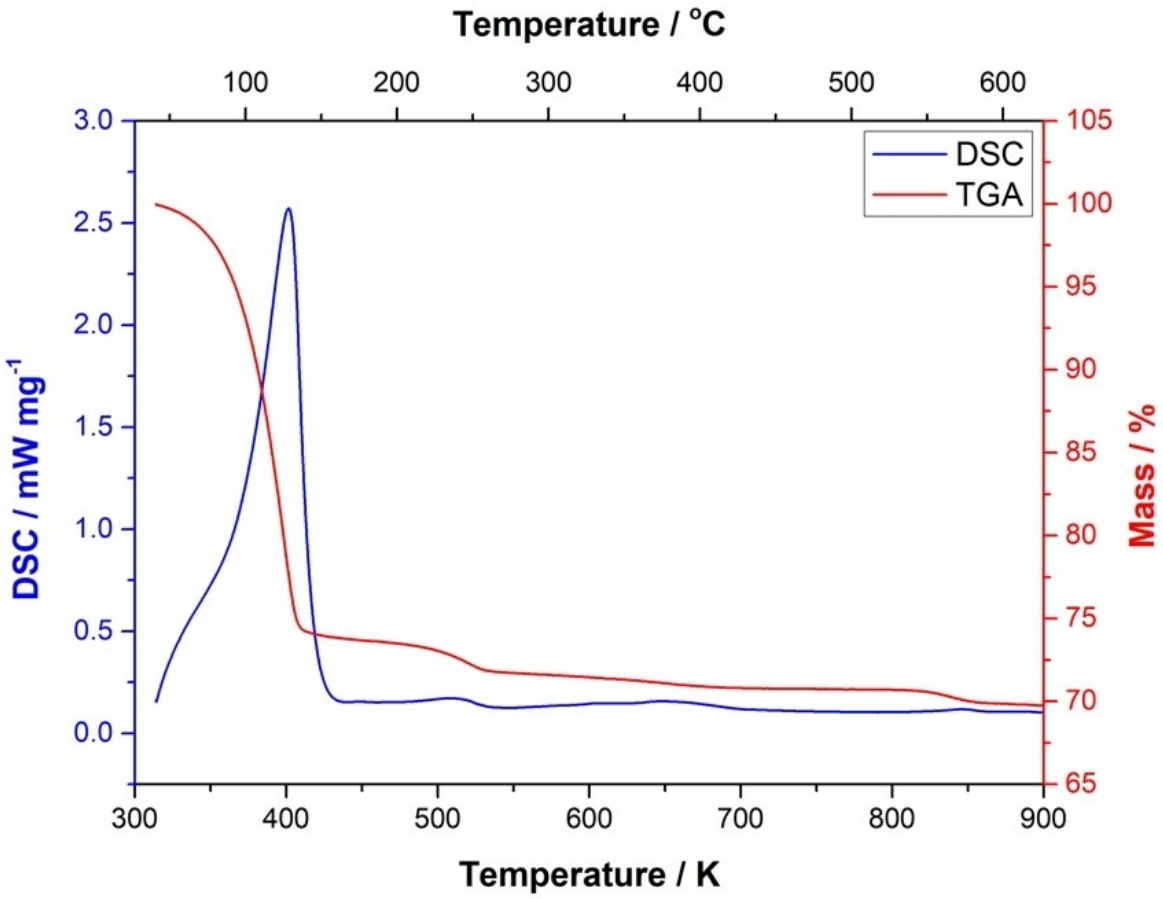

Figure 7. Thermogravimetric analysis (TGA) and differential scanning calorimetry (DSC) curves collected for tetragonal-zircon $BiVO_4$ collected immediately after the coprecipitation reaction. The TGA/DSC data were collected upon heating under a synthetic air (80% N_2, 20% O_2) atmosphere. The blue line corresponds to the DSC, whereas the red line corresponds to the TGA.

ing, the *ts*-$BiVO_4$ structure transforms to the *mf*-$BiVO_4$ polymorph. Although *tz*-$BiVO_4$ can only be isolated using low temperature synthetic methods, crystalline samples of the *mf*-$BiVO_4$ polymorph can be prepared by high temperature solid-state methods. A small anomaly in the thermal expansion of *tz*-$BiVO_4$ was evident between 400–500 K in the high resolution SXRD analysis. This appears to be associated with the loss of H_2O and/or NH_4^+ species that was evident in the combined TGA/FTIR analysis. A remarkable contraction in the V–O bond distance, and of the VO_4 polyhedra volume, was observed upon heating. This is believed to be a consequence of thermally induced rotation of the, essentially, rigid VO_4 tetrahedra.

Attempts to study the structure of *tz*-$BiVO_4$ using neutron diffraction methods were unsuccessful due to the large background that results from the presence of appreciable amounts of hydrogenous species in the sample. Efforts to remove such species whilst maintaining the *tz*-$BiVO_4$ structure failed, suggesting that these may play a role in stabilizing the *tz*-polymorph. XPDF analysis demonstrated that the average structural model provides a good description of the local structure for the *mf*-$BiVO_4$ polymorph, however this was not the case for the *tz*-$BiVO_4$ polymorph. This may simply be a result of local disorder induced by the intercalated H_2O/NH_4^+ species detected by FTIR spectroscopy but may equally point to local scale distortions by the Bi^{3+} 6s^2 lone pair electrons. Neutron total scattering methods would be needed to resolve this, if a suitable deuterated sample could be prepared.

Supporting Information

The electronic supporting information is available free of charge at https://doi.org/10.1002/asia.202400408.

Structural diagrams of the four polymorphs of $BiVO_4$, photos of the synthesis of each $BiVO_4$ polymorph, Rietveld refinements of the synchrotron X-ray diffraction data, variable length range fits of the X-ray pair distribution function data of *tz*- and *mf*-$BiVO_4$, variable temperature neutron diffraction data of *tz*-$BiVO_4$, and thermogravimetric analysis, differential scanning calorimetry, and Fourier transform infrared spectroscopy data.

Acknowledgements

BJK acknowledges the support of the Australian Research Council for this work that was facilitated by access to Sydney

Analytical, a core research facility at the University of Sydney. BGM and MKN acknowledge the Australian Institute for Nuclear Science and Engineering for a scholarship and thank Professor Max Avdeev, as well as Drs Sam Duyker, Majharul Haque Khan, and Michelle Wood for their technical assistance. Part of this work was undertaken at the Powder Diffraction beamline (M18437) at the Australian Synchrotron, at the Echidna and Wombat (P13946) instruments at the Australian Centre for Neutron Scattering, and at Beamline I15-1 at Diamond Light Source (cy30086). Open Access publishing facilitated by The University of Sydney, as part of the Wiley - The University of Sydney agreement via the Council of Australian University Librarians.

Conflict of Interests

The authors declare no conflict of interest.

Data Availability Statement

The data that support the findings of this study are available from the corresponding author upon reasonable request.

Keywords: Phase Transition · Bismuth Vanadate · Photocatalyst · Lone Pair Electrons · X-ray Diffraction

[1] A. Fujishima, K. Honda, *Nature* **1972**, *238* (5358), 37–38.
[2] K. Hashimoto, H. Irie, A. Fujishima, *Jpn. J. Appl. Phys.* **2005**, *44 (12R)*, 8269.
[3] A. Malathi, J. Madhavan, M. Ashokkumar, P. Arunachalam, *Appl. Catal. A* **2018**, *555*, 47–74.
[4] T. D. Nguyen, V.-H. Nguyen, S. Nanda, D.-V. N. Vo, V. H. Nguyen, T. Van Tran, L. X. Nong, T. T. Nguyen, L.-G. Bach, B. Abdullah, *Environ. Chem. Lett.* **2020**, *18*, 1779–1801.
[5] M. Tayebi, B.-K. Lee, *Renewable Sustainable Energy Rev.* **2019**, *111*, 332–343.
[6] I. Vinke, J. Diepgrond, B. A. Boukamp, K. De Vries, A. Burggraaf, *Solid State Ionics* **1992**, *57 (1-2)*, 83–89.
[7] X. Yang, X. Zeng, X. Ming, L. Yang, A. J. Fernández-Carrión, S. Deng, L. He, X. Kuang, *Inorg. Chem. Front.* **2022**, *9* (11), 2644–2658.
[8] S. Sarkar, K. Chattopadhyay, *Phys. E* **2012**, *44 (7-8)*, 1742–1746.
[9] D. Zhou, L.-X. Pang, D.-W. Wang, I. M. Reaney, *J. Mater. Chem. C* **2018**, *6* (35), 9290–9313.
[10] C. Hill, M. C. Weber, J. Lehmann, T. Leinen, M. Fiebig, J. Kreisel, M. Guennou, *APL Mater.* **2020**, *8* (8), 081108.
[11] L. S. Kumari, P. P. Rao, A. N. P. Radhakrishnan, V. James, S. Sameera, P. Koshy, *Sol. Energy Mater. Sol. Cells* **2013**, *112*, 134–143.
[12] N. Sumaletha, K. Rajesh, P. Mukundan, K. Warrier, *J. Sol-Gel Sci. Technol.* **2009**, *52*, 242–250.
[13] Q. Gao, X. Wu, Y. Fan, Q. Meng, *Dyes Pigm.* **2017**, *146*, 537–542.
[14] X. Zhang, T. Chen, Y. Xu, W. Jiang, J. Liu, Z. Xie, *J. Sol-Gel Sci. Technol.* **2019**, *91*, 127–137.
[15] A. W. Sleight, H. Y. Chen, A. Ferretti, D. E. Cox, *Mater. Res. Bull.* **1979**, *14* (12), 1571–1581.
[16] J. Sánchez-Martín, D. Errandonea, J. Pellicer-Porres, D. Vázquez-Socorro, D. Martínez-García, S. N. Achary, C. Popescu, *J. Phys. Chem. C* **2022**, *126* (17), 7755–7763.
[17] M. Qurashi, W. Barnes, *Am. Mineral.* **1953**, *38 (5-6)*, 489–500.
[18] J. D. Bierlein, A. W. Sleight, *Solid State Commun.* **1975**, *16* (1), 69–70.
[19] R. J. Angel, J. Zhao, N. L. Ross, *Phys. Rev. Lett.* **2005**, *95* (2), 025503.
[20] B. J. Kennedy, T. Vogt, C. D. Martin, J. B. Parise, J. A. Hriljac, *Chem. Mater.* **2002**, *14* (6), 2644–2648.
[21] B. J. Kennedy, C. J. Howard, B. C. Chakoumakos, *J. Phys. Condens. Matter* **1999**, *11* (6), 1479.
[22] J. Pellicer-Porres, D. Vázquez-Socorro, S. López-Moreno, A. Muñoz, P. Rodríguez-Hernández, D. Martínez-García, S. N. Achary, A. J. E. Rettie, C. B. Mullins, *Phys. Rev. B* **2018**, *98*, 214109.
[23] X. Cheng, J. Guan, L. Jiang, H. Zhang, P. Wang, A. O. Adeniyi, Y. Yao, L. Su, Y. Song, *Phys. Chem. Chem. Phys.* **2020**, *22*, 10238.
[24] A. K. Bhattacharya, K. K. Mallick, A. Hartridge, *Mater. Lett.* **1997**, *30*, 7.
[25] R. M. Hazen, J. W. E. Mariathasan, *Science* **1982**, *216*, 991.
[26] T. Liu, X. Zhang, J. Guan, C. R. A. Catlow, A. Walsh, A. A. Sokol, J. Buckeridge, *Chem. Mater.* **2022**, *34* (12), 5334–5343.
[27] X. Zhang, Z. Ai, F. Jia, L. Zhang, X. Fan, Z. Zou, *Mater. Chem. Phys.* **2007**, *103* (1), 162–167.
[28] S. Tokunaga, H. Kato, A. Kudo, *Chem. Mater.* **2001**, *13* (12), 4624–4628.
[29] A. Walsh, Y. Yan, M. N. Huda, M. M. Al-Jassim, S.-H. Wei, *Chem. Mater.* **2009**, *21* (3), 547–551.
[30] J. Yu, Y. Zhang, A. Kudo, *J. Solid State Chem.* **2009**, *182* (2), 223–228.
[31] M. W. Stoltzfus, P. M. Woodward, R. Seshadri, J.-H. Klepeis, B. Bursten, *Inorg. Chem.* **2007**, *46* (10), 3839–3850.
[32] A. Polo, I. Grigioni, M. V. Dozzi, E. Selli, *Catal. Today* **2020**, *340*, 19–25.
[33] I. Grigioni, K. G. Stamplecoskie, E. Selli, P. V. Kamat, *J. Phys. Chem. C* **2015**, *119* (36), 20792–20800.
[34] S. P. Berglund, D. W. Flaherty, N. T. Hahn, A. J. Bard, C. B. Mullins, *J. Phys. Chem. C* **2011**, *115* (9), 3794–3802.
[35] W. I. F. David, A. M. Glazer, A. W. Hewat, *Phase Transitions* **1979**, *1* (2), 155–169.
[36] G. Bayer, *J. Less-Common Met.* **1972**, *26* (2), 255–262.
[37] J. Varghese, T. Joseph, K. P. Surendran, T. P. D. Rajan, M. T. Sebastian, D *alton Trans.* **2015**, *44* (11), 5146–5152.
[38] H. L. Li, S. H. Zhou, S. Y. Zhang, *J. Solid State Chem.* **2007**, *180* (2), 589–595.
[39] S. J. Patwe, S. N. Achary, A. K. Tyagi, *Am. Mineral.* **2009**, *94* (1), 98–104.
[40] J. S. O. Evans, T. A. Mary, T. Vogt, M. A. Subramanian, A. W. Sleight, *Chem. Mater.* **1996**, *8* (12), 2809–2823.
[41] F. A. Rabuffetti, S. P. Culver, L. Suescun, R. L. Brutchey, *Inorg. Chem.* **2014**, *53* (2), 1056–1061.
[42] F. P. Marlton, B. G. Mullens, P. A. Chater, B. J. Kennedy, *Inorg. Chem.* **2022**, *61* (38), 15130–15137.
[43] B. G. Mullens, F. P. Marlton, M. Saura-Múzquiz, P. A. Chater, B. J. Kennedy, *Inorg. Chem.* **2024**, *63* (22), 10386–10396
[44] M. Saura-Múzquiz, F. P. Marlton, B. G. Mullens, A. M. Manjón-Sanz, J. C. Neuefeind, M. Everett, H. E. A. Brand, S. Mondal, G. Vaitheeswaran, B. J. Kennedy, *J. Am. Chem. Soc.* **2022**, *144* (34), 15612–15621.
[45] M. Saura-Múzquiz, F. P. Marlton, B. G. Mullens, J. Liu, T. Vogt, H. E. Maynard-Casely, M. Avdeev, D. A. Blom, B. J. Kennedy, *Chem. Mater.* **2023**, *35* (1), 123–135.
[46] B. G. Mullens, F. P. Marlton, M. K. Nicholas, A. J. Permana, M. Avdeev, S. Mukherjee, G. Vaitheeswaran, C. Li, J. Liu, P. A. Chater, B. J. Kennedy, *Inorg. Chem.* https://doi.org/10.1021/acs.inorgchem.4c00866.
[47] K. S. Wallwork, B. J. Kennedy, D. Wang, In *The high resolution powder diffraction beamline for the Australian Synchrotron*, 9th International Conference on Synchrotron Radiation Instrumentation (SRI 2006), Daegu, South Korea, May 28–Jun 02; Daegu, South Korea, **2006**; p 879.
[48] P. Thompson, D. E. Cox, J. B. Hastings, *J. Appl. Crystallogr.* **1987**, *20* (2), 79–83.
[49] M. Basham, J. Filik, M. T. Wharmby, P. C. Chang, B. El Kassaby, M. Gerring, J. Aishima, K. Levik, B. C. Pulford, I. Sikharulidze, *J. Synchrotron Radiat.* **2015**, *22* (3), 853–858.
[50] P. Juhás, T. Davis, C. L. Farrow, S. J. Billinge, *J. Appl. Crystallogr.* **2013**, *46* (2), 560–566.
[51] X. Yang, P. Juhas, C. L. Farrow, S. J. Billinge, *arXiv preprint arXiv:1402.3163* **2014**.
[52] A. C. Larson, R. B. Von Dreele, GSAS. *General Structure Analysis System. LANSCE, MS-H805, Los Alamos, New Mexico* **1994**.
[53] B. H. Toby, *J. Appl. Crystallogr.* **2001**, *34*, 210–213.
[54] A. A. Coelho, *J. Appl. Crystallogr.* **2018**, *51* (1), 210–218.
[55] K. Momma, F. Izumi, *J. Appl. Crystallogr.* **2011**, *44* (6), 1272–1276.
[56] G. Dreyer, E. Tillmanns, *Neues Jahrb. Fur Mineral. Monatshefte* **1981**, *(4)*, 151–154.
[57] V. Sydorchuk, S. Khalameida, N. Shcherban, V. Hreb, V. Mykhaylyk, Y. Zhydachevskyy, L. Vasylechko, *J. Solid State Chem.* **2021**, *296*, 122002.
[58] J. Mariathasan, R. Hazen, L. Finger, *Phase Transitions* **1986**, *6* (3), 165–173.
[59] D. F. Mullica, E. L. Sappenfield, M. M. Abraham, B. C. Chakoumakos, L. A. Boatner, *Inorg. Chim. Acta* **1996**, *248* (1), 85–88.

[60] B. C. Chakoumakos, M. M. Abraham, L. A. Boatner, *J. Solid State Chem.* **1994**, *109* (1), 197–202.
[61] M. Anitha, K. S. Rao, R. Syed, S. Kesari, R. Rao, D. K. Singh, S. N. Achary, V. Kain, *Mater. Chem. Phys.* **2023**, *295*, 127120.
[62] K. Ogawa, R. Abe, A. Walsh, *J. Am. Chem. Soc.* **2024**, *146*(9), 5806–5810.
[63] P. Wood, F. Glasser, *Ceram. Int.* **2004**, *30* (6), 875–882.
[64] B. Noheda, J. Gonzalo, L. Cross, R. Guo, S.-E. Park, D. Cox, G. Shirane, *Phys. Rev. B* **2000**, *61* (13), 8687.
[65] D. Corker, A. Glazer, R. Whatmore, A. Stallard, F. Fauth, *J. Phys. Condens. Matter* **1998**, *10* (28), 6251.
[66] E. S. Božin, C. D. Malliakas, P. Souvatzis, T. Proffen, N. A. Spaldin, M. G. Kanatzidis, S. J. Billinge, *Science* **2010**, *330* (6011), 1660–1663.
[67] T. A. Mary, J. S. O. Evans, T. Vogt, A. W. Sleight, *Science* **1996**, *272* (5258), 90–92.
[68] J. S. Evans, T. Mary, *Int. J. Inorg. Mater.* **2000**, *2* (1), 143–151.
[69] J. Evans, T. Mary, A. Sleight, *J. Solid State Chem.* **1998**, *137* (1), 148–160.
[70] S. P. Culver, R. L. Brutchey, *CrystEngComm* **2016**, *18* (24), 4485–4488.
[71] M. da Silva, L. Dall'Antonia, L. V. d. A. Scalvi, D. dos Santos, L. d. O. Ruggiero, A. Urbano, *J. Solid State Electrochem.* **2012**, *16*, 3267–3274.
[72] M. Li, L. Zhao, L. Guo, *Int. J. Hydrogen Energy* **2010**, *35* (13), 7127–7133.
[73] U. G. Pérez, S. Sepúlveda-Guzmán, A. Martínez-De La Cruz, U. O. Méndez, *J. Mol. Catal. A* **2011**, *335 (1-2)*, 169–175.

Manuscript received: April 13, 2024
Revised manuscript received: May 2, 2024
Accepted manuscript online: May 7, 2024
Version of record online: June 11, 2024